Mon. Not. R. Astron. Soc. **000**, 1–9 (2013) Printed 20 February 2014 (MN LATEX style file v2.2)

The Smith Cloud and its dark matter halo: Survival of a Galactic disk passage

Matthew Nichols[1⋆], Nestor Mirabal[2,3]†, Oscar Agertz[4], Felix J. Lockman[5], Joss Bland-Hawthorn[6]

[1] *Laboratoire d'Astrophysique, École Polytechnique Fédérale de Lausanne (EPFL), Observatoire de Sauverny, 1290 Versoix, Switzerland*
[2] *Ramón y Cajal Fellow*
[3] *Dpto. de Física Atómica, Molecular y Nuclear, Universidad Complutense de Madrid, Spain*
[4] *Department of Physics, University of Surrey, Guildford GU2 7XH, United Kingdom*
[5] *National Radio Astronomy Observatory, P.O. Box 2, Green Bank, WV 24944, United States*
[6] *Sydney Institute for Astronomy, School of Physics, The University of Sydney, NSW 2006, Australia*

ABSTRACT

The current velocity of the Smith Cloud suggests that it has undergone at least one passage of the Galactic disk. We use hydrodynamic simulations to examine the present day structure of the Smith Cloud after it passed through the disk. A dark matter supported cloud is able to reproduce the observed present day structure of the cloud. The dark matter core of a cloud is highly elongated, owing to the gravitational attraction of the disk. We then determine integral flux upper limits to the gamma-ray emission around such a hypothesised dark matter core in the Smith Cloud. No statistically significant core or extended gamma-ray emission are detected down to a 95% confidence level upper limit of 1.4×10^{-10} ph cm^{-2} s^{-1} in the 1–300 GeV energy range. Assuming a distance of 12.4 kpc, the *Fermi* upper limits set the first tentative constraints on the dark matter cross sections annihilating into $\tau^+\tau^-$ and $b\bar{b}$ for a high-velocity cloud (HVC).

Key words: (cosmology:) dark matter – gamma-rays: general – ISM: clouds – ISM: individual objects: Smith cloud – Galaxy: halo

1 INTRODUCTION

The mapping of dark matter substructure around the Galaxy is crucial to understanding how our own Milky Way was assembled over cosmic time. Numerical simulations of the concordant cosmology, dark-energy and cold dark-matter (ΛCDM), predict a multitude of dark-matter subhalos going down in mass to approximately 10^{-4} $M_\odot$ (*e.g.,* Klypin et al. 1999; Moore et al. 1999; Diemand, Kuhlen & Madau 2007; Springel et al. 2008). On the detectable scale of dwarf galaxies, this discrepancy approaches an order of magnitude between the observed dwarf galaxies and the number of predicted subhalos (Mateo 1998; Weinberg et al. 2013). Recent discoveries of ultra-faint dwarf galaxies go someway towards filling this gap (*e.g.,* Willman et al. 2005; Belokurov et al. 2007). Unfortunately, due to the miniscule stellar populations finding these ultra faint dwarfs continues to be challenging and the exact number of them are unknown. The low stellar content of them however, makes them potentially excellent objects to search for dark matter annhilation signals (Charbonnier et al. 2011). So far, no significant detections have yet been made, although upper limits have been placed on the properties of dark matter (*e.g.,* Abdo et al. 2010; Natarajan et al. 2013; The Fermi-LAT Collaboration et al. 2013).

In addition to dwarf galaxies, the Galactic halo contains a large number of intriguing HI substructures in the form of high velocity clouds (HVCs) (Wakker & van Woerden 1997). The suggestion of dark matter surrounding a population of these HVCs has been around for over a decade (*e.g.,* Blitz et al. 1999; Quilis & Moore 2001). Subsequent investigation has determined that any such population is likely to be small in comparison to dark matter free HVCs, both around our own Galaxy (Saul et al. 2012) and also around other galaxies (Chynoweth, Langston & Holley-Bockelmann 2011). Near the disk many of the HVCs are likely to arise through a galactic fountain, where numerous supernova launch gas from the disk of the Galaxy (Bregman 1980). At intermediate distances, within approximately

⋆ E-mail:matthew.nichols@epfl.ch
† E-mail:mirabal@gae.ucm.es

© 2013 RAS

50 kpc, HVCs are likely to originate from the Magellanic Stream and hence originally the LMC and SMC (Putman 2004). Extragalactic HVCs, where they are seen at projected distances exceeding 100 kpc from the nearest galaxy, are likely to be clumps of pristine gas infalling for the first time and possess a phase-space distribution that is incompatible with the expected dark matter substructure (Chynoweth, Langston & Holley-Bockelmann 2011). Despite the abundance of other sources for HVCs, explaining why all dark matter subhalos that failed to form stars lack any gas is difficult and a small fraction of HVCs may be such objects.

In order to investigate the dark matter content in HI clouds, we recently searched for gamma-ray emission from dark matter annihilation at the location of several compact HI clouds in the GALFA-HI Compact Cloud Catalogue (Mirabal 2013). However, poorly constrained astrophysical values, J values, and unknown distances to these objects severly limited our analysis. To advance more throughly, we need to examine systems with better distance determinations and are likely to be candidates for dark matter embedded HVCs. The best candidate for such a search is the Smith Cloud, a massive HI system near the Galactic disk (Smith 1963). The Smith Cloud is an extraordinary gas structure with a cometary tail being accreted onto the Galaxy (Lockman et al. 2008; Nichols & Bland-Hathorn 2009). Unusually for a HVC, the distance to the Smith Cloud is relatively well know (to within 20%). Based on stellar bracketing (Wakker et al. 2008), interaction of stripped material with disk gas (Lockman et al. 2008) and the flux of Hα reflected from the Galactic disk Putman et al. (2003), the distance to the Smith Cloud is known to be 12.4 ± 1.3 kpc (Lockman et al. 2008). Apart from an actual distance estimate, what is particularly appealing about the Smith cloud is that a dark-matter subhalo seems to be required for the survival of the gas cloud after a passage through the Galactic disc (Nichols & Bland-Hathorn 2009).

Given its relative proximity, known orbit and large mass it appears to qualify as the ideal astrophysical site to test the dark matter confinement of HI clouds. Here we search for potential gamma-ray emission from the dark matter annihilation of weakly interacting particles (WIMPs) around the Smith cloud. In Section 2 we present arguments in favour of a dark-matter subhalo surrounding the Smith cloud. Next, we present the *Fermi*-LAT analysis and derive *Fermi* upper limits to the gamma-ray flux. In Section 5, we turn the results into limits on annihilation cross sections. Finally, we summarise our results and present our conclusions.

2 THE SMITH CLOUD AND A DARK MATTER HALO

Most HVCs do not require dark matter to explain their survivability and formation, being able to form through galactic fountains, tidal stripping of gas or condensation of primoridal gas. We argue that none of these processes are likely to be the origin of the Smith Cloud and that a gas cloud encapsulated by dark matter provides the best model for the Smith Cloud.

2.1 Galactic fountains

Compared to most of the HI clouds that surround the Milky Way, the Smith Cloud exceptionally massive, with a mass exceeding 2×10^6 $M_\odot$. Correspondingly, the energy contained in the Smith Cloud is also extremely large compared to the gas at any potential launching point inside the Galactic disk ($\sim 1.0 \times 10^{54}$ erg). This tremendous energy requirement would require of order 1000 supernova in order to produce sufficient energy to dislodge the Smith Cloud inside a galactic fountain. Such a process would also have to take place at a radius $\sim$13 kpc (where its current orbit intersects the disk) in order to be produced (such a simple calculation is in line with a linear scaling of galactic fountain hydrodynamic simulations by de Gouveia Dal Pino et al. 2009). The requirements of a massive cluster at a large radius hence makes it extremely unlikely that the Smith Cloud was formed through any galactic fountain.

If it did not arise directly from the disk, it is still possible to have avoided a disk passage if it had undergone a tidal interaction in the recent past. However, there is no obvious candidate to have provided such a massive cloud and given the paucity of dwarf galaxies that contain gas (Grcevich & Putman 2009), the detection of a suitable host that until recently held gas would raise further questions.

2.2 Passage through the disk

Without arising from the disk and a tidal event being unlikely, the original origin of the Smith Cloud is likely to be from extragalactic infalling gas. Such HVCs are potentially able to survive to near the disk without any dark matter through ablative shielding (Putman, Peek, & Joung 2012; Plöckinger & Hensler 2012). In particular, Plöckinger & Hensler (2012) suggest that dark matter will suppress the characteristic substructure present within HVCs as they approach the disk. However, little work has been done on the passage of HVCs through the disk, potentially the biggest impediment to the survival of the Smith Cloud.

Using the orbital determination of Lockman et al. (2008) the cloud will have passed through the disk approximately 70 Myr ago at a radius of 13 kpc. Such an orbit assumes that drag is minimal along the Smith Clouds orbit, however, given the Smith Cloud's mass, drag is unlikely to have a meaningful impact on the orbit over the last 100 Myr irrespective of any dark matter halo.

At 13 kpc, the surface density of the disk is approximately 3×10^{20} cm^{-2} (Kalberla & Dedes 2008) and is increased by a factor of three due to the oblique angle at which the Smith Cloud passes through the disk. At such high column densities gas clouds passing through the disk are likely to be heavily disrupted. Simple toy models presented in Nichols & Bland-Hathorn (2009) suggest that this disk passage and ram pressure stripping throughout the orbit will require a dark matter halo to survive to the present day.

We supplement the toy model argument presented previously, which suggested a dark matter halo of $M_{\rm tid} \sim 2 \times 10^8$–$1 \times 10^9$ $M_\odot$, with numerical simulations of a cloud passing through a disk with and without a supporting dark matter halo.

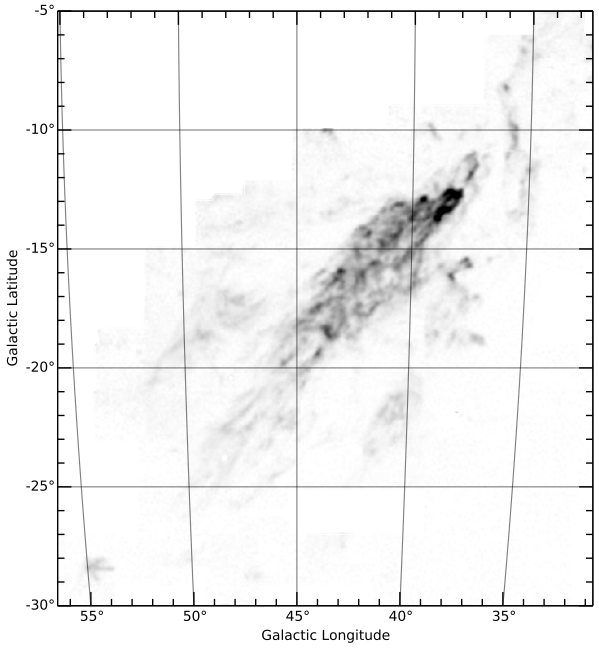

Figure 1. GBT HI image of the Smith Cloud integrated to V_{GSR}=220 km s^{-1} showing the extended cometary morphology of the Smith Cloud.

2.3 HI observations and numerical simulations

In an attempt to replicate the observed structure of the Smith Cloud today, shown in Fig. 1, we use the Adaptive Mesh Refinement (AMR) code RAMSES (Teyssier 2002). The HI 21cm data used here are from a preliminary reduction of a new survey of the Smith Cloud with the 100 meter Green Bank Telescope (GBT) of the National Radio Astronomy Observatory [1]. The new survey covers more than twice the area of the Lockman et al. (2008) survey and uses a different spectrometer that provides four times the velocity resolution (0.32 km s^{-1}) over a 1.6 times greater LSR velocity range, -400 to +400 km s−1 LSR. The preliminary reduction of the new survey data has a median noise level of 65 mK, a factor 1.5 times more sensitive than the previous survey, and the observing and reduction techniques produce maps at the full 9.1 arcmin resolution of the GBT. The new survey is also corrected for residual stray radiation (Boothroyd et al. 2011) improving the dynamic range at low velocities. The new data show that the Smith Cloud is considerably more extended than previously thought, with a diffuse tail to at least l,b = 50,-25 and components that appear to have been detached from the main structure (e.g. at 38,-18 and 40,-22). The observations are nearing completion and the full data set will be published separately.

Using RAMSES we simulate the disk passage of both a dark matter enclosed HI cloud and a dark matter free cloud, along the Smith Cloud's expected orbital path from peak height above the disk 204 Myr ago and compare that to new HI obversations. We include a realistic progenitor to the Smith Cloud and a realistic model of the Milky Way which includes live stellar and gaseous disks and dark matter halo. We evolve the coupled N-body and hydrodynamical system while accounting for metal dependent radiative cooling and UV background heating as per Agertz (2013) at a maximum resolution of $\Delta x \sim 30$ pc.

The Smith Cloud progenitor is modelled as a constant density ($n = 0.1$ cm^{-3}) 10^7 $M_\odot$, HI cloud, such a cloud is approximately three times bigger than the Smith Cloud today, but in line with massive clouds in nearby systems (*e.g.,* Chynoweth et al. 2008) as well as allowing a large degree of mass loss to the present day. In order to model the survival with and without a dark matter halo, we consider both a pressure supported cloud and one which is embedded within an NFW dark matter halo of virial mass $M_{\rm NFW} = 3 \times 10^8$ $M_\odot$ and concentration $c = 30$.

The model galaxy is considered to consist of a galactic disk of total mass $M_{\rm disk} = 4.3 \times 10^{10}$ $M_\odot$, where the gaseous disk accounts for 8.6×10^9 $M_\odot$ of the baryons. The disk has a scale radius of $r_{\rm disk} = 3.4$ kpc and an exponential scale height $h = 0.1 r_{\rm disk}$. These disks are embedded inside a hot gaseous halo with density $n = 10^{-4}$ cm^{-3} along with a $M_{\rm vir} = 10^{12}$ $M_\odot$ NFW dark matter halo with concentration $c = 10$. Note that the adopted gaseous halo density, out to the initial simulation cloud altitude ($z \sim 20$ kpc) 204 Myr ago, is a *conservative* choice, as the observed circum-disk medium likely is denser; Gaensler, Madsen, Chatterjee, & Mao (2008) found that a warm gaseous disk of the form $n(z) = n_0 \exp(-z/H)$, where $n_0 = 0.014$ cm^{-3} and $H = 1.8$ kpc, is consistent with the Milky Way.

We use the preliminary results from new HI observations and the resulting HI intensity from the simulations (as would be observed today) in Fig. 2 and the line of slight velocity in Fig. 3 to examine the structure of the cloud. Overlaid the observed HI of the Smith Cloud and the simulated dark matter confined cloud are contours representing the surface density of the resulting dark matter. Both simulated clouds survive the passage through the disk and subsequent passage through the the hot halo. However, the dark matter free cloud loses coherency, becoming mixed with the gas from the hot halo and loses the substructure present within the cloud. In contrast, the HVC embedded inside a dark matter halo retains this dense core of gas, similar to the compact 'head' of the Smith Cloud. We plot the mass weighted probability density function in Fig. 4, and see that while the HVC which lacks dark matter rarely exceeds a density of 2.5 cm^{-2}, the dark matter embedded cloud retains a dense core exceeding 10 cm^{-2} which would be observed as a high column density core on the sky.

Due to the added gravitational attraction of the baryonic disk the dark matter core of the HVC becomes significantly elongated (flatenning of ∼1/2 in the case examined here). Such a transformation from a spherical halo to a roughly prolate spheroid differs from the expected result from dark matter only simulations, where tidal forces tend to make a subhalo more spherical (Moore, Kazantzidis, Diemand, & Stadel 2004).

2.4 Dark matter properties

Given the above problems for a dark matter free Smith Cloud, the assumption of an encapsulating dark matter halo

[1] The National Radio Astronomy Observatory is a facility of the National Science Foundation operated by Associated Universities, Inc.

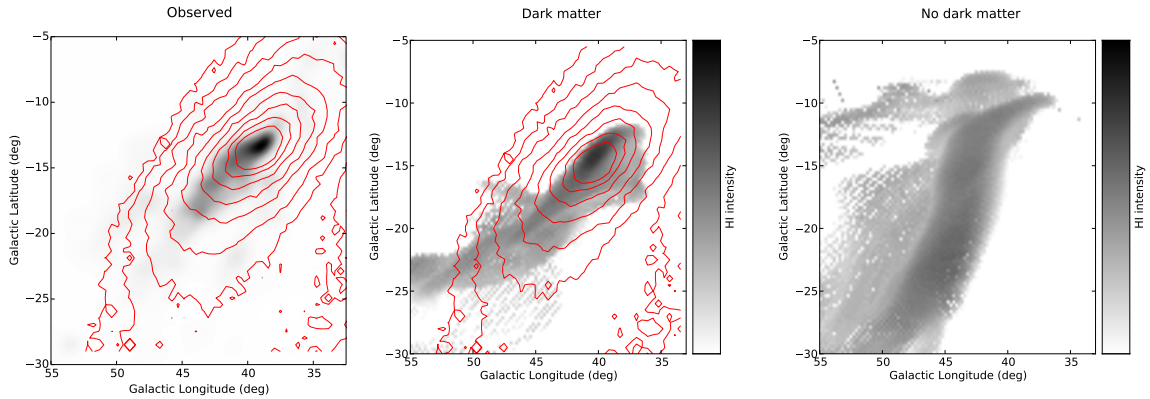

Figure 2. Smoothed Smith Cloud HI observations with simulated dark matter contours (left) [dark matter contours offset by (-0.5°,1°) to better fit the cloud], and simulated HI intensity for a HVC that has passed through the Galactic disk, encapsulated by dark matter (centre) or without dark matter (right). The dark matter contours are shown in (red) solid lines and represent the average line of sight density between 10^8 $M_\odot$ kpc^{-3} and 10^6 $M_\odot$ kpc^{-3} in 0.25 dex steps. While the cloud encapsulated by dark matter still shows substructure, this is erased in the dark matter free case where the cloud loses coherence and smooths out.

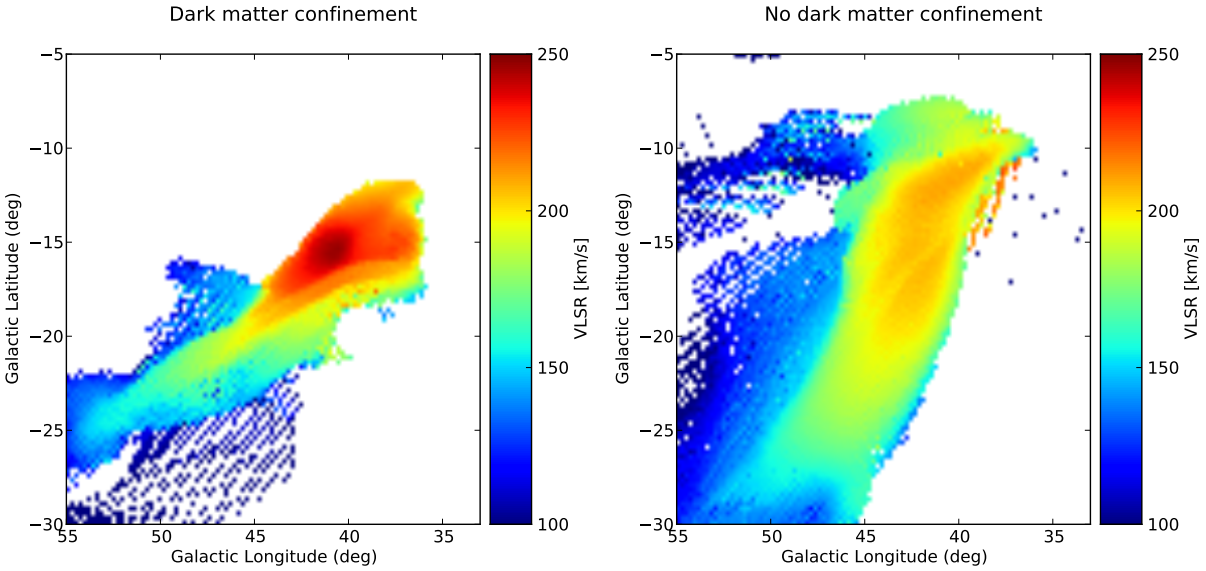

Figure 3. HI $V_{\rm LSR}$ for a HVC that has passed through the Galactic disk, encapsulated by dark matter (left) or without dark matter (right). The cloud encapsulated by dark matter retains a gradient as is observed in the present day Smith Cloud (although at a slightly higher velocity) while this gradient disappears in the dark matter free case.

remains a viable hypothesis. The properties of the dark matter halo can be estimated from the above conditions. If the halo is not massive enough it will face the same problems as a dark matter free cloud. If it is too massive, the potential well will have enabled star formation to take place inside the core of the Smith Cloud, something for which there is no evidence.

Analytic limits are explored in Nichols & Bland-Hathorn (2009) which, for an NFW profile, gives limits corresponding to a dwarf galaxy sized dark matter halo $M_{\rm vir} = 10^9$ $M_\odot$, although this may vary by at least a factor of 3. Such a halo corresponds to $r_s \sim$ 1–1.8 kpc and $\rho_s \sim 6 \times 10^6$–$2 \times 10^7$ $M_\odot$ kpc^{-3}.

3 FERMI-LAT OBSERVATIONS AND ANALYSIS

To search for gamma-ray emission associated with the Smith cloud, we use *Fermi*-LAT observations carried out between 2008 August 4 to 2013 June 11 (4.85 years of data), corresponding to the interval from 239557417 and 392621346 in Mission Elapsed Time (MET). The analysis is performed using the `v9r27p1` *Fermi* Science Tools together with the standard `P7SOURCE_V6` instrument response function. In order to minimise contamination by the Earth's limb we exclude events with zenith angles $> 100°$. We also filter the data using the `gtmktime` filter expression recommended by the LAT team, namely "(DATA_QUAL==1) && (LAT_CONFIG==1) && ABS(ROCK_ANGLE)<52". Fig. 5 shows photon count maps for 100 MeV – 1 GeV and

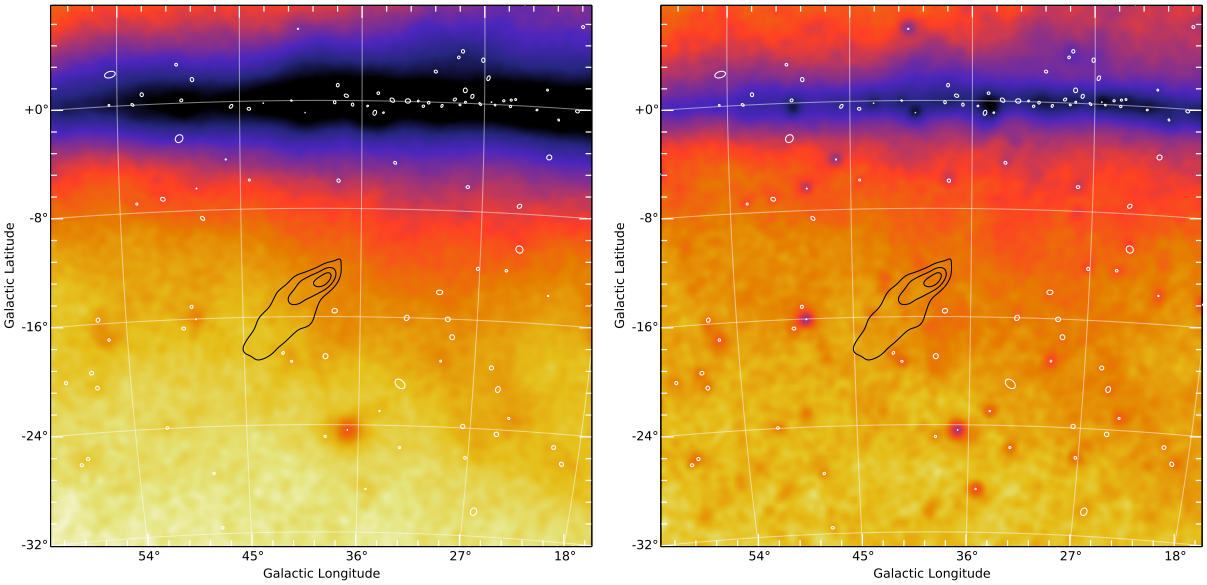

Figure 5. Smoothed *Fermi*-LAT count maps of a 40° × 40° region around the simulated Smith Cloud for 100 MeV–1 GeV (*left*) and 1–300 GeV (*right*) respectively. Radio contours for the Smith Cloud are overlaid in green. As the dark matter halo closely follows the HI distribution, this is also approximately the expected dark matter location. The white symbols pinpoint 95% confidence ellipses of 2FGL point sources (Nolan et al. 2012).

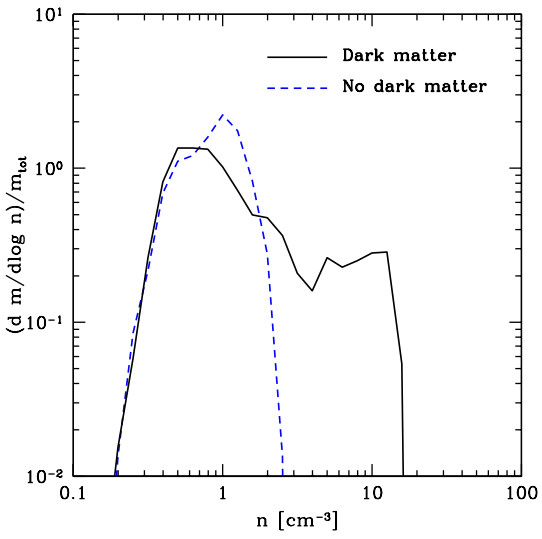

Figure 4. Mass weighted probability density function of HI density within the Smith Cloud. While the dark matter embedded HVC retains a dense core (observed as the dark HI clump in Fig. 2, the dark matter free cloud contains contains only low to medium density gas unlike the smith cloud today.

1 – 300 GeV with contours of integrated HI emission from the Smith Cloud superimposed in green. With the current *Fermi* data, we do not see any obvious morphological correspondence between the gamma-ray emission and the HI cometary morphology reported by Lockman et al. (2008).

An interesting possibility is that there may be additional spatially extended emission due to dark matter stripped off during the cloud's history. In order to constrain such scenario, we sum gamma-ray counts over the entire orbit of the Smith cloud. The orbit is calculated using the potential from Wolfire (1995) as detailed in (Nichols & Bland-Hathorn 2009). The estimated trajectory is given in 1 Myr steps in Table 1. We consider photons within ±1° along the orbit, roughly corresponding to the 95% containment angle of the *Fermi* LAT for energies above 10 GeV. Point and and extended 2FGL sources listed in Nolan et al. (2012) are masked since they can contaminate the actual cloud contribution. The counts are then compared with the observed counts in the anti-orbit of the cloud, corresponding to the same Galactic longitude but with opposite sign in Galactic latitude. Compared to its anti-orbit, we find no statistically significant gamma-ray excess in the orbit for energies above 1 GeV. The presence of gamma-ray point sources present along the vicinity of the orbit masks important portions of the trajectory, but at present this seems the only reasonable procedure.

Given the absence of extended gamma-ray emission, events are only extracted within a 10° radius centred on the current position of the hypothesised dark matter subhalo core at $(\ell, b) = (38.5°, -13.4°)$. This final step, in practice, assumes that the subhalo has retained its integrity during the orbit, which the simulations suggest is likely. The dataset is analysed using the binned likelihood method, implemented as the `gtlike` tool in the standard *Fermi* Science

Tools[2]. At the position of the Smith cloud, we create a count map within our region of interest (ROI) with `gtbin`. We then generate a binned exposure map with `gtexpcube2`, and a model source/diffuse count map with `gtsrcMaps`. In order to place an upper limit for the integrated photon flux, we take advantage of the implementation of `LATAnalysisScripts`[3]. Upper limits are computed with `calcUpper` assuming a power law spectrum with photon index $\Gamma = 2$. The 95% confidence upper limit in the 1–300 GeV energy range is 1.4 $times10^{-10}$ ph cm^{-2} s^{-1}.

4 BOUNDS ON DARK MATTER CROSS SECTIONS

Our next task is to translate the derived *Fermi* upper limits into actual constraints on annihilation cross sections. In order to so, we use the predicted gamma-ray flux from dark matter annihilation (Baltz et al. 2008) that can be written as

$$\Phi_\gamma(E_\gamma, \Delta\Omega) = \Phi^{\rm PP}(E_\gamma) \times J(\Delta\Omega)\,, \qquad (1)$$

where $\Phi^{\rm PP}(E_\gamma)$ is the "particle physics factor" that measures the number of gamma-ray photons per dark matter annihilation. The quantity J is the "astrophysical factor" which depends on the integral of the dark matter distribution $\rho_{\rm DM}$ over the line of sight l. According to this model,

$$J = \int_{\Delta\Omega}\int \rho^2_{\rm DM} l, \Omega)\, {\rm d}l{\rm d}\Omega. \qquad (2)$$

Here, the solid angle $\Delta\Omega$ as a function of the integration angle $\alpha_{\rm int}$ is defined as

$$\Delta\Omega = 2\pi \cdot (1 - \cos(\alpha_{\rm int}))\,. \qquad (3)$$

As emphasised previously, since we do not know actually know where in the orbit of Smith the dark-matter subhalo is located, we are making the simplified assumption – supported by simulations – that it is still mostly intact at the head of the cometary structure after its passage of the Galactic disk. We can then estimate J assuming the values for the dark matter distribution from Section 2. All calculations of J presented therein have been obtained with the `CLUMPY` package (Charbonnier, Combet & Maurin 2012). For the dark-matter subhalo, we consider a canonical Navarro-Frenk-White (NFW) profile (Navarro, Frenk & White 1996),

$$\rho_{NFW}(r) = \rho_s \left(\frac{r}{r_s}\right)^{-1} \left[1 + \left(\frac{r}{r_s}\right)\right]^{-2}. \qquad (4)$$

where ρ_s is the scale density, and r_s is the scale radius. For the actual computation, we adopt $\rho_s = 1.5 \times 10^7$ M$_\odot$ kpc^{-3} and $r_s = 1.04$ kpc from Nichols & Bland-Hathorn (2009). Integrating with $\alpha_{\rm int} = 0.1^\circ$ (used throughout the text) which is compatible with the *Fermi*-LAT PSF at energies > 1 GeV, we find $\log_{10} J_{NFW} = 18.44$ GeV^2 cm^{-5}.

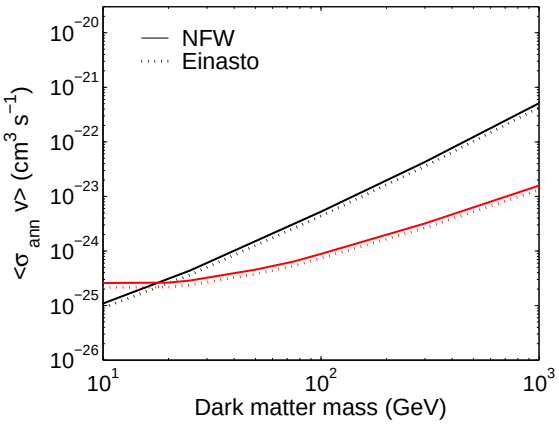

Figure 6. Derived upper limits for $\langle\sigma v\rangle_\chi$ versus dark matter mass for both the NFW and Einasto profiles. $\tau^+\tau^-$ (black) and $b\bar{b}$ (red) channels are shown.

To allow for a different spatial model, we can also calculate the dark matter distribution with an Einasto profile (Einasto 1965; Springel et al. 2008) of the form,

$$\rho_{Einasto}(r) = \rho_{-2} \exp\left\{-\frac{2}{\alpha}\left[\left(\frac{r}{r_{-2}}\right)^\alpha - 1\right]\right\}, \qquad (5)$$

where r_{-2} marks the radius where the slope of the profile equals the isothermal value $\gamma = 2$. We assume the scalings provided by Navarro et al. (2010) so that $r_{-2} = r_d$, and $\rho_s = 4\rho_{-2}$ respectively. This increases the value of the astrophysical value slightly to $\log_{10} J_{Einasto} = 18.52$ GeV^2 cm^{-5}.

Referring back to Baltz et al. (2008), we can write the particle physics term $\Phi^{\rm PP}(E_\gamma)$ as

$$\Phi^{\rm PP}(E_\gamma) \equiv \frac{{\rm d}\Phi_\gamma}{{\rm d}E_\gamma} = \frac{1}{4\pi}\frac{\langle\sigma v\rangle}{2m^2_\chi} \times \sum_f \frac{{\rm d}N_\gamma}{{\rm d}E_\gamma} B_f, \qquad (6)$$

where $\langle\sigma v\rangle_\chi$ is the averaged annihilation cross section times the relative velocity, m_χ is the dark matter particle mass, ${\rm d}N_\gamma/{\rm d}E_\gamma$ is the photon yield per annihilation final state f, and B_f is the branching ratio. For our calculations of ${\rm d}N_\gamma/{\rm d}E_\gamma$, we use the analytical fits to `PYTHIA` simulation spectra provided in Fornengo, Pieri & Scopel (2004). We only consider dark matter annihilating into τ-lepton pair ($\tau^+\tau^-$) and bottom quark ($b\bar{b}$) final states. Fig. 6 shows the cross section upper limits as a function of dark matter mass for both channels.

5 DISCUSSION AND CONCLUSIONS

We have undertaken analytic calculations and numeric simulations to investigate whether the Smith Cloud is encapsulated within a dark matter halo. Without a dark matter halo, the passage of a HVC through the disk of the Galaxy is likely to remove any substructure, resulting in a cloud substantially different to the observed Smith Cloud. With dark matter the HVC is able to survive the passage and retain substantial substructure and resulting in a cloud which looks similar to the Smith Cloud today. Such simulations suggest

[2] http://fermi.gsfc.nasa.gov/ssc/data/analysis/scitools/binned_likelihood_tutorial.html
[3] http://fermi.gsfc.nasa.gov/ssc/data/analysis/scitools/LATAnalysisScripts.html

that the idea of the Smith Cloud being encapsulated by a dark matter halo remains plausible.

We report photon flux upper limits for the gamma-ray emission at the current position of the Smith Cloud using 4.85 years of accumulated *Fermi*-LAT data to investigate the properties of such a dark matter halo. We exclude WIMPs annihilating into $\tau^+\tau^-$ and $b\bar{b}$ final states down to $\langle\sigma v\rangle_\chi \sim 3\times10^{-25}$ cm^3 s^{-1} for masses around 10 GeV. The obvious caveat is that dark matter might have been shed during the history of the cloud, however, the simulations have the dark matter retain the cloud core up to its present day location with only minor elongation. To investigate this case in any case we compare the counts from orbit and anti-orbit, we find no evidence for excess gamma-ray emission along the predicted trajectory of the cloud system. In addition, there is no morphological gamma-ray structures overlapping the cometary structure reported in HI.

The velocity averaged annihilation cross section upper bounds obtained around the Smith cloud are compatible with limits from other searches reported in the dwarf galaxies (Abdo et al. 2010) and galaxy clusters (Ackermann et al. 2010). Our results rest upon the assumption that there is indeed a dark-matter subhalo seeding the Smith Cloud. To this extent we undertook simulations demonstrating that such an assumption is plausible given the disk passage the Smith Cloud is likely to have undertaken. As well as demonstrating that the Smith Cloud's structure can be reproduced through a dark matter embedded HVC, such a result suggests that clouds with dark matter that have passed a disk may take on the comet like morphology observed in expected in DM free HVCs which have not yet crossed the disk (*e.g.,* Putman, Saul, & Mets 2011; Plöckinger & Hensler 2012). The latter still needs to be verified with future observations, however, it provides potentially the best candidate for a dark matter confined HVC. Despite this failed effort, gamma-ray observations still offers one of the few available opportunities to diagnose the dark matter content of gaseous clouds. Upcoming experiments such as the Cherenkov Telescope Array (CTA) it will make it possible to achieve improved angular resolution and sensitivity around the Smith Cloud for energies above 100 GeV (CTA Consortium 2013; Doro et al. 2013).

ACKNOWLEDGMENTS

N.M. acknowledges support from the Spanish taxpayers through a Ramón y Cajal fellowship and the Consolider-Ingenio 2010 Programme under grant MultiDark CSD2009-00064. All numerical simulations were conducted on the RCC Midway cluster at the University of Chicago. OA is grateful to Doug Rudd for making the use of the Midway cluster a smooth experience. We thank Tarek Hassan for his help with general technicalities.

REFERENCES

Abdo A. A. et al. 2010, ApJ, 712, 147
Ackermann M. et al. 2010, JCAP, 05, 025
Agertz, O., Kravtsov, A. V., Leitner, S. N., & Gnedin, N. Y. 2013, ApJ, 770, 25
Baltz E. A. et al. 2008, JCAP, 7, 13
Belokurov V. et al. 2007, ApJ, 654, 897
Blitz L., Spergel D. N., Teuben P. J., Hartmann D., Burton W. B. 1999, ApJ, 514, 818
Boothroyd, A. I., Blagrave, K., Lockman, F. J., Martin, P. G., Pinheiro Gonçalves, D., & Srikanth, S. 2011, A&A, 536, A81
Bregman J. N. 1980, ApJ, 236, 577
Charbonnier, A., et al. 2011, MNRAS, 418, 1526
Charbonnier A., Combet C., Maurin D. 2012, Comp. Phys. Comm., 183, 656
Chynoweth, K. M., Langston, G. I., Yun, M. S., Lockman, F. J., Rubin, K. H. R., & Scoles, S. A. 2008, AJ, 135, 1983
Chynoweth, K. M., Langton, G. I., Holley-Bockelmann, K. 2011, AJ, 141, 9
CTA Consortium 2013, Astrop. Phys., 43, 3
Diemand, J., Kuhlen, M., Madau, P. 2007, ApJ, 667, 859
Doro M. et al. 2013, Astrop. Phys., 43, 189
Einasto J. 1965, Trudy Inst. Astroz. Alma-Ata, 51, 87
Fornengo N., Pieri L., Scopel S. 2004, Phys. Rev. D, 70, 103529
Gaensler, B. M., Madsen, G. J., Chatterjee, S., & Mao, S. A. 2008, PASA, 25, 184
de Gouveia Dal Pino, E. M., Melioli, C., D'Ercole, A., Brighenti, F., & Raga, A. C. 2009, RMxAC, 36, 17
Grcevich, J., & Putman, M. E. 2009, ApJ, 696, 385
Kalberla, P. M. W., & Dedes, L. 2008, A&A, 487, 951
Klypin A., Kravtsov A. V., Valenzuela O., Prada F. 1999, ApJ, 522, 82
Lockman F. J., Benjamin R. A., Heroux A. J., Langston G. I. 2008, ApJ, 679, L2
Maloney P. R., Putman M. E. 2003, ApJ, 589, 270
Mateo M. 1998, ARA&A, 36, 435
Mirabal N. 2013, MNRAS, 432, 71
Moore B. et al. 1999, ApJ, 524, L19
Moore, B., Kazantzidis, S., Diemand, J., & Stadel, J. 2004, MNRAS, 354, 522
Natarajan, A., Peterson, J. B., Voytek, T. C., Spekkens, K., Mason, B., Aguirre, J., & Willman, B. 2013, PhRvD, 88, 083535
Navarro J. F., Frenk C. S., White S. D. M. 1996, ApJ, 462, 563
Navarro J. F. et al. 2010, MNRAS, 402, 21
Nichols M., Bland-Hawthorn J. 2009, ApJ, 707, 1642
Nolan P. L. et al. 2011, ApJS, 199, 31
Oort J. H. 1970, A&A, 7, 381
Plöckinger, S., & Hensler, G. 2012, A&A, 547, A43
Putman, M. E., Bland-Hawthorn, J., Veilleux, S., Gibson, B. K., Freeman, K. C., & Maloney, P. R. 2003, ApJ, 597, 948
Putman, M. E. 2004, ASSL, 312, 101
Putman, M. E., Saul, D. R., & Mets, E. 2011, MNRAS, 418, 1575
Putman, M. E., Peek, J. E. G., & Joung, M. R. 2012, ARA&A, 50, 491
Quilis, V., Moore, B. 2001, ApJ, 555, L95
Saul, D. R., et al. 2012, ApJ, 758, 44
Springel V. et al. MNRAS, 391, 1685
Smith G. P. 1963, Bull. Astron. Inst. Neth., 17, 203
Teyssier, R. 2002, A&A, 385, 337
The Fermi-LAT Collaboration, et al. 2013, arXiv, arXiv:1310.0828

Wakker B. P., van Woerden H. 1997, ARA&A, 35, 217
Wakker, B. P., York, D. G., Wilhelm, R., Barentine, J. C., Richter, P., Beers, T. C., Ivezić, Ž., & Howk, J. C. 2008, ApJ, 672, 298
Weinberg D. H., Bullock J. S., Governato F., Kuzio de Naray R., Peter A. H. G. 2013, preprint (arXiv:1306.0913)
Willman B. et al. 2005, ApJ, 626, L85
Wolfire M. G., McKee C. F., Hollenback D., Tielens A. G. G. M. 1995, ApJ, 453, 673

Table 1. Predicted orbit of the Smith cloud over the next 40 Myr.

Step (Myr)	ℓ	b
1	20.66	4.62
2	20.94	4.36
3	21.24	4.09
4	21.53	3.82
5	21.84	3.54
6	22.14	3.24
7	22.46	2.94
8	22.78	2.63
9	23.10	2.31
10	23.44	1.98
11	23.77	1.64
12	24.12	1.29
13	24.47	0.92
14	24.83	0.55
15	25.20	0.16
16	25.57	-0.24
17	25.95	-0.65
18	26.34	-1.06
19	26.74	-1.49
20	27.15	-1.92
21	27.56	-2.37
22	27.99	-2.82
23	28.43	-3.28
24	28.87	-3.75
25	29.33	-4.22
26	29.80	-4.71
27	30.27	-5.21
28	30.77	-5.71
29	31.27	-6.23
30	31.78	-6.76
31	32.31	-7.30
32	32.86	-7.85
33	33.42	-8.41
34	33.99	-8.99
35	34.58	-9.58
36	35.19	-10.18
37	35.81	-10.79
38	36.46	-11.42
39	37.12	-12.07
40	37.80	-12.73
41	38.51	-13.42